



hal-00400387, version 1 - 30 Jun 2009

1 Quasistatic displacement self-sensing method for cantilevered 2 piezoelectric actuators

3 Ioan Alexandru Ivan, Micky Rakotondrabe,^{a)} Philippe Lutz, and Nicolas Chaillet
 4 *Department of Automatic Control and Micro-Mechatronic Systems, FEMTO-ST Institute,*
 5 *UMR CNRS 6174-UFC/ENSM/UTBM, 24 rue Alain Savary, 25000 Besançon, France*

6 (Received 27 March 2009; accepted 4 May 2009; published online xx xx xxxx)

7 Piezoelectric meso- and microactuator systems required for manipulation or assembly of microscale
 8 objects demand reliable force and/or displacement information. Available sensors are prone to
 9 dimension restrictions or precision limitation. Self-sensing method, based on the electric charge
 10 measurement, may represent a solution in terms of cost-effectiveness and integration, the actuator
 11 performing simultaneously as its own sensor. This paper presents a self-sensing method dedicated
 12 to free uni- and bimorph piezocantilevers but can also be adapted to other piezoactuator types. The
 13 integrated electric current, used to convert the charge, can be compensated against piezoelectric
 14 material nonlinearities to provide accurate displacement information. The advantages relative to
 15 existing self-sensing methods consist in the ability to keep this displacement information for
 16 long-term periods (more than a thousand seconds) and in the reduction in signal noise. After
 17 introductory issues related to the method the base principle allowing the estimation of tip
 18 displacement is presented. Then, the identification procedure of the estimator parameters is depicted
 19 and representative experimental results are shown. Finally, a series of aspects related to electronic
 20 circuits are discussed, useful for successful system implementation.
 21

22 I. INTRODUCTION

23 Piezoelectric cantilevered actuators usually made up of
 24 one or two piezoelectric layers (called uni- or bimorph) are
 25 present in many micromanipulation and microrobotic appli-
 26 cations, thanks to their high displacement resolution and fast
 27 response time. The static and dynamic behaviors of piezo-
 28 electric actuators, their inherent nonlinearities (hysteresis and
 29 creep), and limits were studied and modeled¹⁻⁴ especially
 30 during the past 2 decades in attempting to provide more ef-
 31 ficient control solutions.⁵⁻⁷

32 In order to perform very accurate and fast response time
 33 closed-loop micromanipulation tasks, various sensors have
 34 been used. Unfortunately, these sensors are not ideally
 35 adapted to the micro- and nanoworld because of their sizes,
 36 performances, and limited measurement of degrees of free-
 37 dom. Table I summarizes mostly available sensors in the
 38 field. Hence, an alternative to the use of sensors is the self-
 39 sensing method. There are several advantages of the self-
 40 sensing method relative to the use of external sensors.
 41 Among them, it allows a consistent reduction in the costs by
 42 eliminating expensive sensors. As can be seen, resolution can
 43 also be submicrometric and comparable to that of external
 44 sensors. Self-sensing is based on charge conversion. In fact,
 45 charge is nearly proportional to the displacement, hence
 46 there is no need to further compensate the complex nonlin-
 47 earities (hysteresis and creep) such as in (Ref. 8).

48 The idea of self-sensing in piezoelectric cantilever has

been started by the work of Dosch *et al.*⁹ While it is not a
 new concept on vibration damping or control,¹⁰⁻¹³ more re-
 cently, it has shown its feasibility for piezoelectric tubes of
 atomic force microscopy.^{14,15} But to our knowledge, self-
 sensing methods have not yet been adapted for long-term
 (more than hundreds of seconds) displacement measurement
 of cantilevered actuators, as required by micromanipulation
 and microrobotic tasks. In this paper, we present a compen-
 sated self-sensing approach especially dedicated to long-term
 static measurement. We especially focus on the displacement
 measurement of a piezoelectric cantilever beam.

Drawbacks of displacement self-sensing method refer to
 inherent charge leaks and temperature influence. With proper
 actuators and electronic circuits, charge information may be
 preserved even for thousands of seconds. However, because
 of the temperature variations, extra care will be required for
 proper thermal isolation especially in the case of nonsym-
 metric cantilevers (example: unimorph) to limit temperature-
 related uncertainties.

There are several self-sensing schematics depending on
 application. Capacitive bridges^{9,11} are convenient for vibra-
 tion control but are not easy to balance for long-term mea-
 surements. Structures with both electrodes for actuation and
 electrodes for sensing are a simple solution but their incon-
 venience is a partial reduction in the total actuating
 range.^{14,16} A current integrator was introduced in Ref. 17 for
 a piezostack. The disadvantage was a poor compensation of
 leaking resistance with a very high value potentiometer
 across the integrating capacitor. Another method quite relat-
 ed to self-sensing concept was linearization of the actuator
 displacement using voltage-to-charge amplifiers.^{18,19} The ad-

^{a)}Author to whom correspondence should be addressed. Electronic mail:
 mrakoton@femto-st.fr.

TABLE I. Displacement sensors for the microworld.

Sensor type	Advantages	Disadvantages
Triangulation lasers	High precision and resolution; fair band pass; and spot measurement	Quite expensive, large sizes, and limited measurement range
Interferometers	Very high precision resolution and range; increased band pass; and spot(s) measurement	Very expensive and large sizes
Diffraction grating target	High precision and multidimensional measurement	Large sizes, require attaching target, and expensive
Strain gages	Less expensive and millimeter size	Fragile, noisy output signal, and temperature influence
Capacitive or inductive	High sensibility, high precision, and fair price	Require linearization, from fair to quite large dimensions, and close vicinity requirements
Magnetic Hall effect, magnetoresistive, and magnetostrictive	Good precision, band pass, and fair price	Require permanent magnets often too large and close vicinity requirements.
Using image processing	Large measurement range and in-plane displacement	Expensive and limited resolution and response time
<i>Piezoelectric self-sensing</i>	Double functionality, high band pass, high resolution, and lowest price	Require nonlinear compensation and long-term charge leaking

80 vantage was a linear voltage-to-displacement characteristic.
 81 However, the conventional HV supplier needs to be replaced
 82 by more complex charge driven circuits. In our paper we
 83 propose two simple schematics of current integrators (modi-
 84 fied charge amplifiers) that can also be easily implemented
 85 onto existing systems, avoiding requiring the redesign of ac-
 86 tuator or HV supply.

87 The developed self-sensing systems can be divided into
 88 three main parts, as in Fig. 1: the piezoelectric actuator, the
 89 electronic circuit, and the data processing system. The latter
 90 is the proposed self-sensing estimator. The estimate displace-
 91 ment could be used for further feedback or closed-loop con-
 92 trol systems.

93 Piezoelectric actuators are submitted to V_{in} external volt-
 94 ages in a range of up to several hundred volts, depending on
 95 actuators. Resulted charge Q (in fact integrated current) is
 96 converted by the electronic amplifier to a measurable voltage
 97 V_{out} . This signal will be converted for further numerical pro-
 98 cessing. Data is further processed on a computer or is de-
 99 ployed into a real-time processor or microcontroller. External
 100 signals can be provided to improve the self-sensing accuracy,
 101 for instance temperature variation may be compensated with
 102 a small thermistor. As the charge cannot be kept indefinitely,
 103 external resetting before each measurement prevents satura-
 104 tion and offsets large parts of the static error.

105 Among the contributions of this paper include: the intro-
 106 duction of an antiparallel reference capacitance, numerical
 107 compensations of amplifier bias currents and of piezoelectric
 108 leaking resistance, and dielectric absorption. A step by step
 109 approach of the identification of the self-sensing parameters
 110 is presented as well as experimental results.

111 The paper is organized as follows. First, we present the
 112 principle and related equations of the self-sensing estimator.

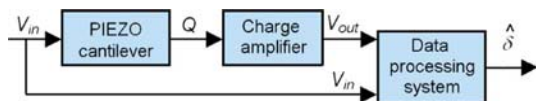


FIG. 1. (Color online) Displacement self-sensing system.

Afterwards, we detail the parameter identification. Hence, we
 present the experimental results. Finally, we relate some is-
 sues to be taken into account when deploying self-sensing
 systems.

II. DISPLACEMENT DETECTION

A. Charge output of piezoelectric cantilever

Consider a bimorph cantilevered beam piezoactuator
 subjected to an electrical excitation V_{in} (Fig. 2). The beam is
 characterized by its length L , its width w , and its half-
 thickness h .

In the absence of external force, we have a theoretically
 linear relation between displacement and applied voltage²⁰

$$\delta = - \frac{3d_{31}}{d_{31}^2} \frac{L^2}{h^2} V_{in}, \quad (1)$$

where s_{11}^E is the compliance coefficient along the beam (X
 direction), ϵ_{33}^S and d_{31} are dielectric and piezoelectric mate-
 rial coefficients.

Using the relation between the applied voltage and the
 capacitance for bimorph piezoelectric cantilever beam

$$Q = \frac{4wL\epsilon_{33}^S}{h} V_{in}, \quad (2)$$

charge directly results and, as stated previously, is quasipro-
 portional to free displacement δ

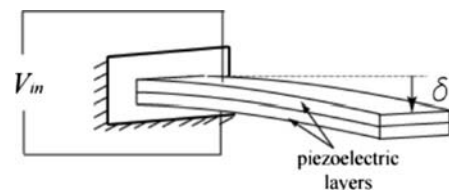


FIG. 2. A bimorph piezoelectric cantilever beam.

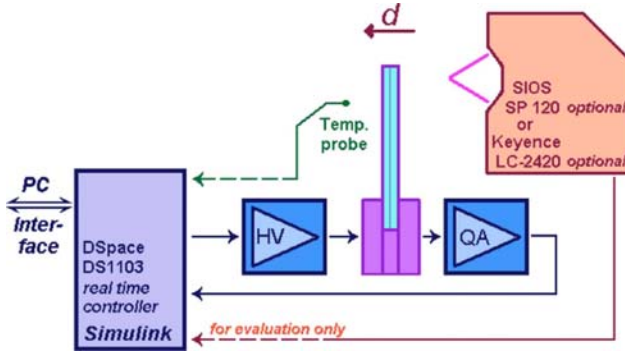


FIG. 3. (Color online) Experimental setup schematic of the self-sensing actuator. Direction for positive displacement is given.

$$Q = \frac{4whe_{33}^S}{3d_{31}L} \left(1 + \frac{d_{31}^2}{4s_{11}^E \epsilon_{33}^S} \right) \delta = \alpha \delta, \quad (3)$$

where α is denoted as an actuator charge-displacement coefficient. In the sequel, this charge will be converted into a measurable voltage V_{out} from which the deflection δ will be estimated, as described in Fig. 1.

B. Experimental setup

A schematic overview of the setup is depicted in Fig. 3. Several uni- and bimorph rectangular actuators (PZT on Cu or Ni substrate) were tested, of length between 10–15 mm, width between 1–2 mm, and total thickness of 0.27–0.45 mm. A Keyence LC-2420 optical displacement reader was only used for intermediate tests on actuators displacement; for some measurements requiring better precision a SIOS SP-120 miniature plane-mirror interferometer was employed (Fig. 4). However displacement readings served only for referencing and evaluating purposes of the self-sensing method. The high voltage (HV) amplifier allowed applying a voltage up to ± 150 V. A current integrator amplifier circuit (modified charge amplifier) to be discussed next chapter provided V_{out} output signal. The Matlab Simulink detection model was deployed on a high speed DSpace DS1103 real-time controller board. A PC-based CONTROLDESK interface served for model parameterization and data acquisition/presentation.

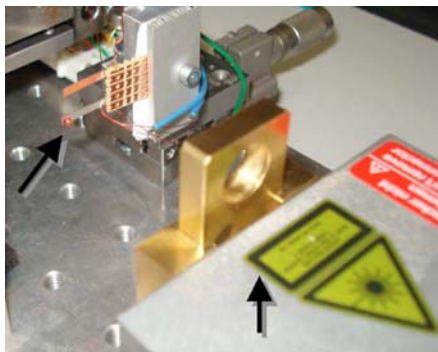


FIG. 4. (Color online) Photo of experimental setup. Actuator is placed in the upper left and SIOS interferometer is in the right side of the image.

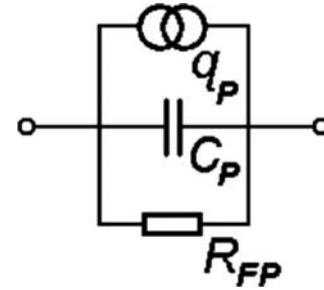


FIG. 5. Equivalent electrical schematic of a piezoactuator.

C. Integrator amplifier

The static electrical equivalent schematic of piezoelectric bender is a charge generator in parallel with a capacitor and a leaking resistance, as seen in Fig. 5, and its electromechanical model is shown in Ref. 2. C_p capacitance is in the order of nanofarad depending on the shape and dimensions of the microactuator's structure while R_{FP} is the insulating resistance, whose order of magnitude is between $10^9 \dots 10^{12} \Omega$.

If we ignore nonlinear effects, charge is proportional to the applied voltage and the external force. To measure charge, we propose a precise integrator circuit scheme, as pictured in Fig. 6 and described below.

The input signal V_{in} is inverted and applied to a “reference capacitor” C_R whose the value is close to C_p value; it will “absorb” a significant part of the charge due to the applied voltage, according to the second Kirchoff law. Although C_R and HV inverter may miss from the circuit, their use is recommended. Indeed, the output will saturate at a higher V_{in} input voltage value (up to several hundred volts) while preserving the same sensitivity. Feedback capacitor C will integrate the current due to external force variation and applied voltage (depending on C_R/C_p fraction). An electro-mechanical relay-switch k (in series with several kilo ohms resistor) allows resetting V_{out} voltage from DSpace environment in order to avoid the saturation. Electronic switches are not suitable because of their “off” source/drain leakage currents. Further details and propositions are discussed in Sec. V.

Output voltage is

$$V_{out} = -\frac{1}{C} \int_0^T i(t) dt = -\frac{1}{C} Q, \quad (4)$$

where, for the free beam ($F_{ext}=0$), charge is

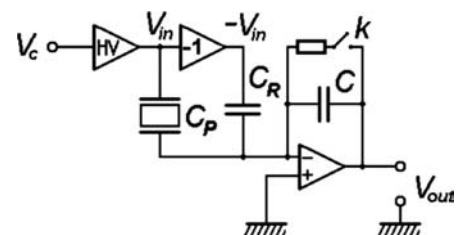


FIG. 6. Electronic circuit schematic of charge amplifier.

157

158

159

160

161

162

163

164

165

166

167

168

169

170

171

172

173

174

175

176

177

178

179

180

181

182

183

184

185

186

187

188

189

190

191

192

193

194

195

196

197

198

199

200

201

202

203

204

205

206

207

208

209

210

211

212

213

214

215

216

217

218

219

220

221

222

223

224

225

226

227

228

229

230

231

232

233

234

235

236

237

238

239

240

241

242

243

244

245

246

247

248

249

250

251

252

253

254

255

256

257

258

259

260

261

262

263

264

265

266

267

268

269

270

271

272

273

274

275

276

277

278

279

280

281

282

283

284

285

286

287

288

289

290

291

292

293

294

295

296

297

298

299

300

301

302

303

304

305

306

307

308

309

310

311

312

313

314

315

316

317

318

319

320

321

322

323

324

325

326

327

328

329

330

331

332

333

334

335

336

337

338

339

340

341

342

343

344

345

346

347

348

349

350

351

352

353

354

355

356

357

358

359

360

361

362

363

364

365

366

367

368

369

370

371

372

373

374

375

376

377

378

379

380

381

382

383

384

385

386

387

388

389

390

391

392

393

394

395

396

397

398

399

400

401

402

403

404

405

406

407

408

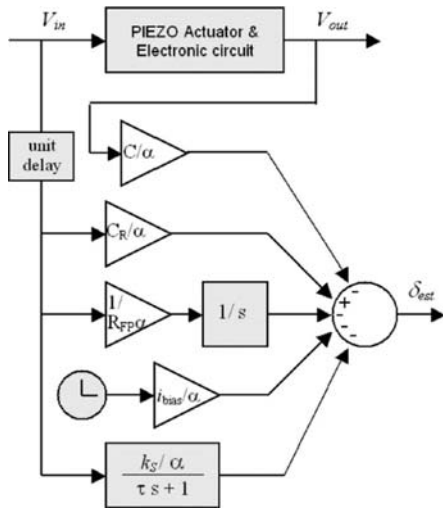


FIG. 7. Displacement detection model (Simulink).

$$Q = -C_R V_{in} + \alpha \delta, \quad (5)$$

where α was introduced in Eq. (3).

If we consider a nonlinear dielectric absorption effect of piezoelectric material, we propose the following slight modification:

$$Q = -C_R V_{in} + (\alpha \delta + Q_{DA}), \quad (6)$$

where Q_{DA} is an internal amount of charge depending on ϵ_{33} variation.

D. Detected displacement formula

Adding the influence of the nonzero bias current i_{BIAS} of the operational amplifier (op-amp) and finite leaking resistance R_{FP} of the piezoactuator, output voltage V_{out} of the free cantilever beam is given by

$$V_{out} = \frac{C_R}{C} V_{in} - \frac{\alpha \delta + Q_{DA}}{C} - \frac{1}{C} \int \frac{V_{in}(t)}{R_{FP}} dt - \frac{1}{C} \int i_{BIAS}(t) dt. \quad (7)$$

Extracting the displacement δ , we obtain the estimate as follows:

$$\delta_{est} = -\frac{C}{\alpha} V_{out} - \frac{Q_{DA}(V_{in}, t)}{\alpha} + \frac{C_R}{\alpha} V_{in} - \frac{1}{R_{FP} \alpha} \int V_{in}(t) dt - \frac{1}{\alpha} \int i_{BIAS}(t) dt. \quad (8)$$

We will consider a simple relaxation effect described by a first-order transfer function for the dielectric absorption term

$$Q_{DA}^*(s) = \frac{Q_{DA}(s)}{\alpha} = \frac{k_s^*}{\tau s + 1}, \quad (9)$$

where static gain $k_s^* = k_s / \alpha$. Based on the previous equations, Fig. 7 presents the detailed estimation bloc-scheme. Some parameters of the identification in Eq. (8) have to be identified. It will be presented in the next section.

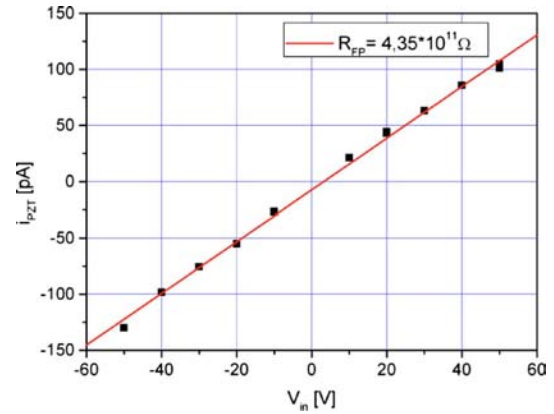


FIG. 8. (Color online) Leakage current of PZT actuator measured under constant dc voltage values. Calculated insulation resistance is 0.435 T Ω .

III. SELF-SENSING PARAMETER IDENTIFICATION

Parameters identification of Eq. (8) can be performed under a manual or semiautomatic procedure. Capacitances are given ($C=47$ nF and $C_R=8.2$ nF in our case). The identification procedure for the rest of parameters (α , i_{BIAS} , R_{FP} , and Q_{DA}) is based on Eq. (7), where the displacement δ is provided by the displacement sensor (optical or interferometer). The following steps describe the identification procedure.

A. Bias current i_{BIAS} identification

Under $F_{ext}=0$, $V_{in}=0$, $V_{out} \cong 0$, and zero temperature change, there is no electric current through the piezoelectric material; the V_{out} rate of change is measured for several dozens of seconds, deriving i_{BIAS} .

B. Leaking resistance R_{FP} identification

Under $F_{ext}=0$, a constant voltage $V_{in} \neq 0$ is applied to the actuator. After several hundred seconds the creep influence becomes negligible, and the output voltage V_{out} shifts with a constant slope, depending on i_{BIAS} (identified before) and R_{FP} (to be identified).

The identification can be repeated for different V_{in} values and averaged. Each point in Fig. 8 was recorded after a 1000–2000 s delay, to eliminate residual creep influence. Linear regression was applied.

Quality piezocantilevers will exhibit R_{FP} values superior to 1010 Ω . For our actuator we identified $R_{FP}=0.435$ T Ω .

C. Displacement coefficient α identification

A step signal is applied on the free actuator. To avoid dynamic oscillations of the actuator, the step signal is shaped with ramp of around 20 V/s (Fig. 9). Measured values of δ and V_{out} immediately after V_{in} step signal will serve to compute α

$$\alpha = (-C V_{out} + C_R V_{in}) / \delta. \quad (10)$$

An alternate method for deriving α is to apply one or several sinusoidal signals as in Fig. 10 and use amplitude values in Eq. (10).

215

216

217

218

219

220

221

222

223

224

225

226

227

228

229

230

231

232

233

234

235

236

237

238

239

240

241

242

243

244

245

246

247

248

249

250

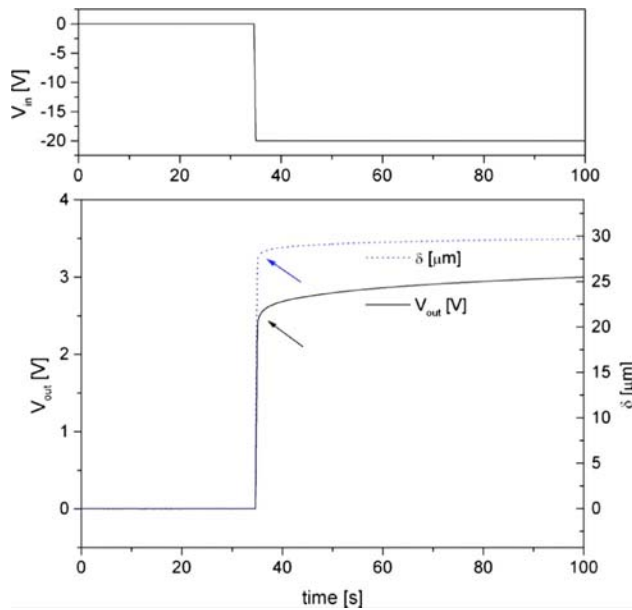


FIG. 9. (Color online) Identification of α coefficient with a -20 V ramped step input.

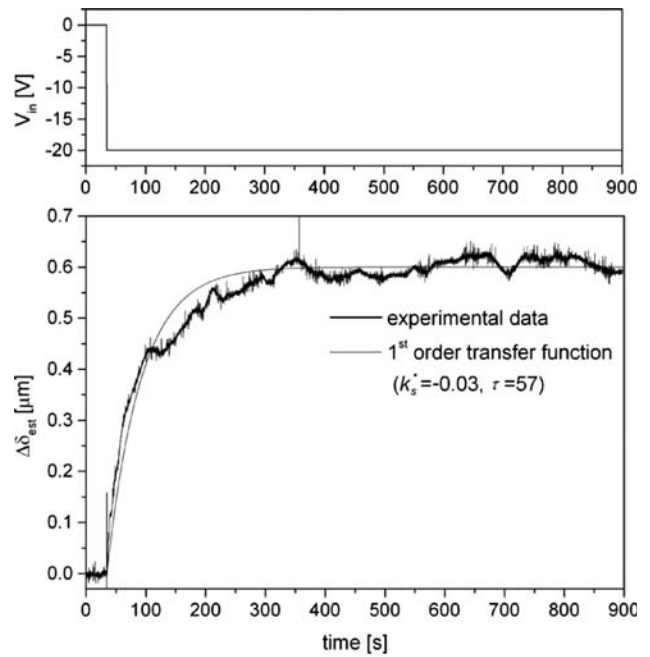


FIG. 11. Identification of dielectric absorption $Q_{DA}^*(s)$ transfer function.

251 D. Identification of dielectric absorption transfer 252 function

253 The last part to be identified in displacement in Eq. (8) is
254 the dielectric absorption $Q_{DA}(V_{in}, t)$ of the piezoelectric
255 material.

$$256 \quad \Delta \delta_{est}(s) = Q_{DA}^*(s) V_{in}(s), \quad (11)$$

257 where $\Delta \delta_{est} = \delta_{est} - \delta$ is the difference between estimated (us-
258 ing already identified parameters) and measured tip displac-
259 ements (Fig. 11). Identification of k_s and τ is performed on a
260 step response, calculating the static gain and response time to
261 reach 63.2% of final value.

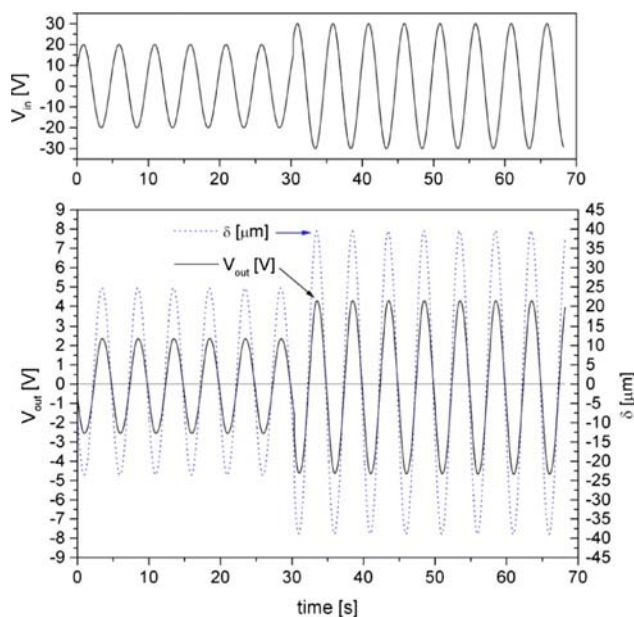


FIG. 10. (Color online) Identification of α coefficient from sinusoidal signals.

IV. SELF-SENSING RESULTS

Several tests have been performed to evaluate the accu-
racy of the proposed self-sensing technique. Known and
identified parameters are entered into the real-time processor,
we have

$$\alpha = -10.05e^{-9} \text{ C/m},$$

$$C = 47e^{-9} \text{ F},$$

$$C_P = 1.74e^{-9} \text{ F},$$

$$C_R = 8.2e^{-9} \text{ F},$$

$$R_{FP} = 0.435e^{12} \Omega,$$

$$i_{BIAS} = -1.7e^{-12} \text{ A},$$

$$\tau = 57 \text{ s},$$

$$k_s = 3.02e^8 \text{ m/V}.$$

A. Displacement self-sensing results

In Fig. 12, an input signal V_{in} was applied in several
steps between $+20$ and -25 V, under null external force.
Data was recorded for 1020 s—largely sufficient for most
applications involving piezoelectric actuators. A very good
agreement is found; measured and detected displacement
curves almost superpose.

A comparative representation of displacement errors is
made as follows. Three graphs are traced (Figs. 13–15) from
uncompensated to fully compensated with respect to leaking
resistance and dielectric absorption. Measurement with Key-
ence optical displacement reader provided a poorer linearity
than self-sensing signal, making it impossible for accurate
error evaluation; SIOS interferometer was eventually em-

262

263

264

265

266

267

268

269

270

271

272

273

274

275

276

277

278

279

280

281

282

283

284

285

286

287

288

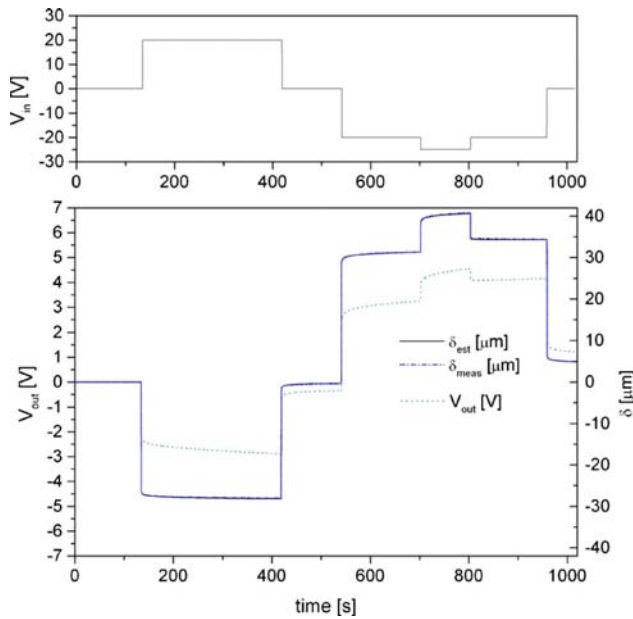


FIG. 12. (Color online) Measured and detected displacement for an arbitrary V_{in} input signal ($F_{ext}=0$).

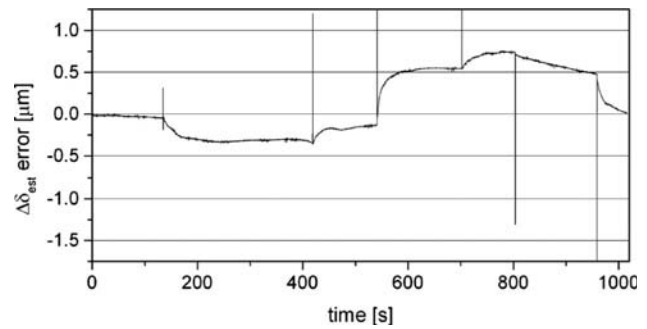


FIG. 14. Error curve of detected displacement with only leaking resistance R_{FF} compensation.

piezoelectric and passive material tend to bend the structure like a thermal bimetallic, conducting to parasitic displacement (and charges). In this case Eq. (2) between charge and displacement no longer applies ($Q \neq \alpha \delta$), leading to displacement errors. To analyze the thermal influence, we compared its effects on two types of piezoelectric beams: unimorph and bimorph cantilevers. As seen in figures and as expected, unimorphs (Fig. 17) are more affected by ambient temperature than bimorphs (Fig. 18). As bimorph cantilevers are intrinsically symmetric, charges from both sides sum up and self-compensate.

If we compare the above results, we see that unimorph cantilevers are five times more sensitive to temperature than bimorphs. Errors can be limited by a proper thermal isolation or compensated with a sensitive temperature sensor like a miniature thermistor. However, temperature sensor should be in contact with the actuator for more correlate readings.

V. CURRENT INTEGRATION RELATED ISSUES

An improper choice of charge amplifier²¹ will significantly reduce sensing accuracy. The circuit should be protected against temperature changes, with a special care to PCB design (guard rings, sufficient space between routes, vias, and pads) otherwise unwanted leakage will easily exceed op-amp bias current.

Integrating capacitor must have primarily an extremely high insulation resistance, low dissipation factor, and good temperature stability. Polypropylene plastic film capacitors were employed in our case, with a measured leaking resistance of 24 TΩ for $C=10$ nF, high enough to ignore its

289 ployed. Our constraint on the utilized interferometer is that
 290 data is only available offline. Vertical error lines in the fig-
 291 ures can be neglected and are due to the linear interpolation
 292 and sampling period mismatch between the two data sets
 293 (acquired at sampling rates of 10 and 16.11 Hz).
 294 As seen in the Fig. 13, peak-to-peak error of uncompen-
 295 sated signal is $2.75 \mu\text{m}$. Compensation of R_{FF} leaking resis-
 296 tance allowed a reduction in maximum error to $1.05 \mu\text{m}$
 297 (Fig. 14). Adding the compensation of dielectric absorption
 298 (Fig. 15) provided a $0.38 \mu\text{m}$ (0.55%) peak-to-peak error.
 299 Unaveraged measured self-sensing signal noise in dis-
 300 placement is of only 1.6 nm (rms), being 10 times less noisy
 301 than that of filtered Keyence LC-2420 sensor (16.7 nm rms
 302 noise on 4096 averaged samples). However, as expected,
 303 SIOS SP 120 interferometer showed best results: 0.5 nm rms
 304 noise (Fig. 16).

305 B. Temperature influence on displacement self- 306 sensing accuracy

307 Temperature exhibits changes in dielectric and piezo-
 308 electric constants. Also, differences in thermal expansion of

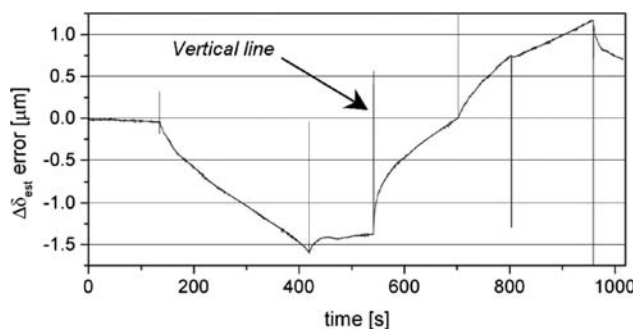


FIG. 13. Error curve of detected displacement with no leaking resistance R_{FF} and dielectric absorption Q_{DA} compensation.

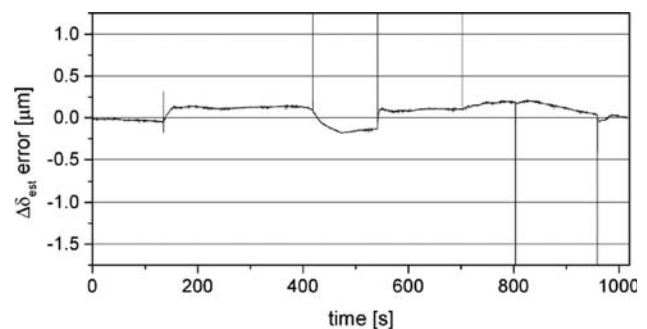


FIG. 15. Error curve of detected displacement with compensation of leaking resistance R_{FF} and dielectric absorption Q_{DA} .

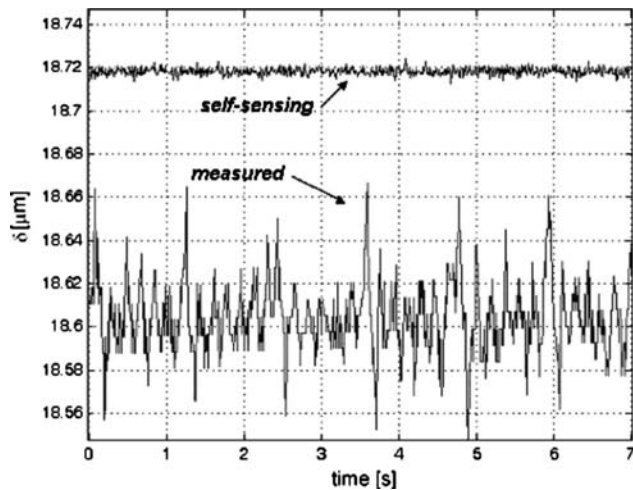


FIG. 16. Zoomed in measure (Keyence LC2420) and detected displacement for noise evaluation.

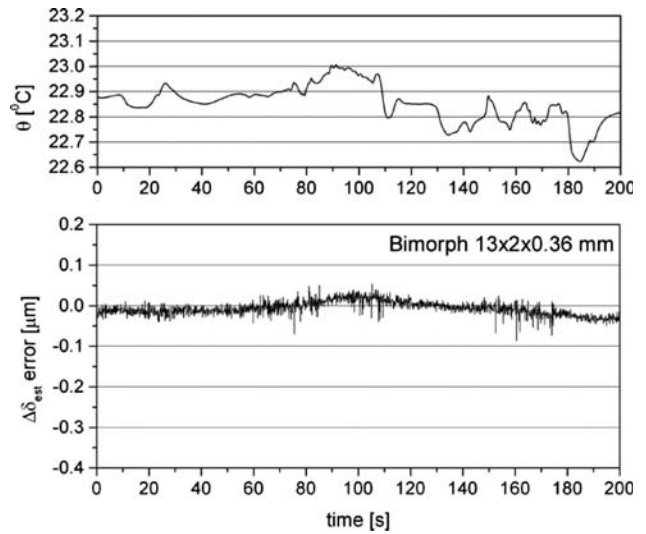


FIG. 18. Typical self-sensing displacement error due to ambient temperature change in a bimorph actuator. Error is $\sim 0.2 \mu\text{m}/^\circ\text{C}$.

338 leaking influence in the circuit. Polystyrene or Teflon capaci-
339 tors also showed better performance than ceramic or polyes-
340 ter film capacitors.

341 Precise operational amplifiers used in charge amplifiers
342 must be unity-gain stable; otherwise they will tend to oscil-
343 late. Noise and bias currents have to be as small as possible.
344 Several op-amp types were tested, OPA111BM Difet model
345 was chosen for its very small bias current (1.7 pA), small
346 offset voltage, small temperature drift, fair supply voltage,
347 and on-chip guarding ring. OPA627 model is also suitable.

348 Attention has must be paid to supply and input voltages.
349 The circuit is damaged if high input voltage is applied in the
350 absence of supply voltage. Also, to prevent the output satu-
351 ration, the k switch allows resetting when necessary. Further
352 increase in voltage over an already saturated op-amp will
353 cause damage.

354 Cables should be shielded properly to avoid the electro-
355 magnetic interference. Further noise rejection can be
356 achieved by modifying the electronic schematic presented in

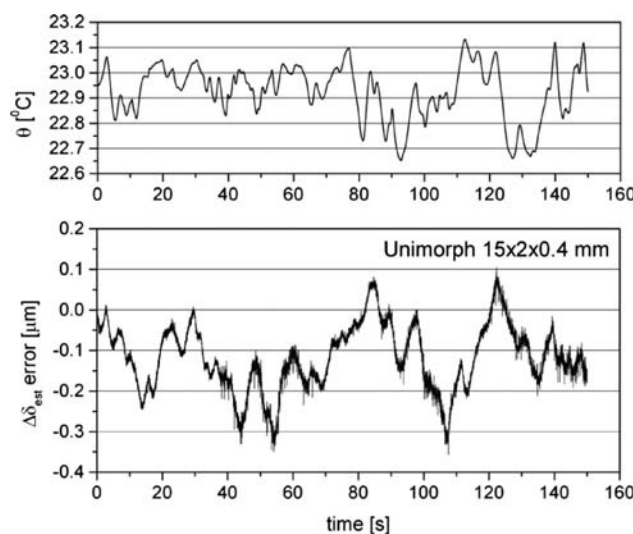


FIG. 17. Typical self-sensing displacement error due to ambient temperature change in a unimorph actuator. Error is $\sim 1 \mu\text{m}/^\circ\text{C}$.

Fig. 6. We propose the schematic pictured in Fig. 19 where
the current, proportional to the voltage drop across a series
resistance or more likely across a voltage divider (to avoid
op-amp damage due to HV), is buffered or preamplified and
then integrated. Indeed, this schematic allows noise reduction
thanks to the grounded series resistance R_{Z_2} connected to
the high impedance amplifier input.

$$V_{\text{out}} = - \frac{R_{Z_2}}{RC(R_{Z_1} + R_{Z_2})} \int_0^T i(t) dt, \quad (12)$$

For our actuator the best compromise between response time,
sensitivity, and noise was a series resistance of 82 k Ω (R_{Z_1}
+ R_{Z_2} = 82 k Ω).

Noise was reduced by a factor of five but on the other
hand this schematic was much more sensitive to temperature
offset drifts than that of Fig. 6. As V_z voltage is in the μV
range or lower, op-amp offset voltage temperature drift
($\pm 0.5 \mu\text{V}/^\circ\text{C}$) and supply rejection ($\pm 3 \mu\text{V}/\text{V}$) limited
system accuracy. Usually op-amp offset is trimmed manually
(with potentiometers); in our case this measure was not suf-
ficient to compensate thermal drifts. We made an automatic
compensation of the offset voltage with random temperature
changes. This was performed by connecting DSpace DAC
outputs (Fig. 20) to op-amp “trim” pins and by measuring
and referencing the temperature to a miniature thermistor in
close contact with op-amp chip. This way, we preserved a
signal up to 100 s similar in accuracy with that of Figs.
12–15, however rms noise was reduced from 1.6 nm to only
0.4 nm, inferior to even that of SIOS SP120 interferometer.

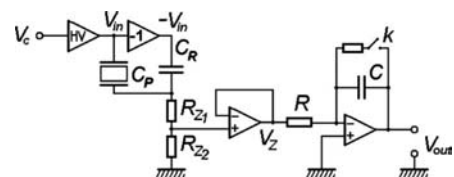


FIG. 19. Alternate schematic with voltage divider and integrator allowed noise reduction.

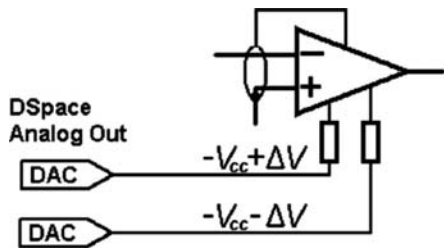


FIG. 20. Offset drift compensation connecting DSpace output to trim pins.

384 Zero-drift chopper op-amps (typically $\pm 0.03 \mu\text{V}/^\circ\text{C}$) will
 385 probably ameliorate temperature drifts but other effects such
 386 as thermal electro motive force (EMF) (Seebeck effect) in
 387 cable junctions will still perturbate the circuit.

388 To generally resume, charge integration is prone to non-
 389 zero bias currents offset voltages, temperature drifts, leaking
 390 resistance or currents, thermal EMF and electro magnetic
 391 interference influence. However, with proper measures, their
 392 influence can be eliminated or at least partially quantified
 393 and compensated.

394 VI. CONCLUSION

395 Displacement self-sensing of uni- and bimorph cantile-
 396 vered actuators used for meso- and microscale gripping and
 397 manipulation is cost-effective and relatively simple to imple-
 398 ment or upgrade to existing systems. To our knowledge it is
 399 a first paper focusing on displacement self-sensing of these
 400 devices. We referred to a current integration method self-
 401 compensated against some actuator nonlinearities (hysteresis
 402 and creep) and externally compensated to others (leaking re-
 403 sistivity and dielectric absorption).

404 In the case of detected or *a priori*—supposed absence of
 405 external forces, displacement is almost directly proportional
 406 to the charge. Further compensation of nonzero amplifier
 407 bias current, finite actuator leaking resistance, and dielectric
 408 absorption lead to a significant reduction in errors, up to
 409 0.55% and an increase in measurement period to more than
 410 1000 s, sufficient enough for most tasks. Signal noise was
 411 lower than that measured with expensive laser triangulation
 412 sensor. Two schematics were presented, the first one based
 413 on direct current integration showed its feasibility for long
 414 integration periods while the second integrating shunt volt-
 415 age drop allowed a further reduction in signal noise with a

cost of a more unstable long-term signal. Practical issues
 related to long-term charge preservation were presented, and
 temperature influence discussed.

ACKNOWLEDGMENTS

The authors especially thank Roger Bourquin, professor
 at ENSMM Besancon, France, for helpful discussions. This
 work is supported by the EU FP7 SP3-People Program under
 Grant No. PIEF-GA-2008-219412 (New Micro-Robotic
 Systems featuring Piezoelectric Adaptive MicroStructures
 for Sensing and Actuating, with Associated Embedded
 Control).

- ¹T. S. Low and W. Guo, *J. Microelectromech. Syst.* **4**, 230 (1995). 427
- ²H. J. M. T. A. Adriaens, W. L. de Koning, and R. Banning, *IEEE/ASME Trans. Mechatron.* **5**, 31 (2008). 428
- ³Y.-G. Zhou, Y.-M. Chen, H.-J. Ding, and W.-Q. Chen, *J. Zhejiang Univ. Sci. A.* **9**, 1 (2008). 429
- ⁴M. Rakotondrabe, Y. Haddab, and R. S. Fearing, Proceedings of the IEEE International Conference on Robotics and Automation, Spain, 2005 (unpublished). 430
- ⁵H. Jung and D.-G. Gweon, *Rev. Sci. Instrum.* **71**, 1896 (2000). 431
- ⁶M. Rakotondrabe, C. Clévy, and P. Lutz, *IEEE Trans. Autom. Sci. Eng.* (unpublished). 432
- ⁷M. Rakotondrabe, Y. Haddab, and P. Lutz, *IEEE Trans. Control Syst. Technol.* **17**, 528 (2009). 433
- ⁸M. Rakotondrabe, Y. Haddab, and P. Lutz, Proceedings of the IEEE/ASME International Conference on Advanced Intelligent Mechatronics, Zurich, Switzerland, September 2007 (unpublished), pp. 1–6. 434
- ⁹J. J. Dosch, D. J. Inman, and E. Garcia, *J. Intell. Mater. Syst. Struct.* **3**, 166 (1992). 435
- ¹⁰W. W. Law, W.-H. Liao, and J. Huang, *Smart Mater. Struct.* **12**, 720 (2003). 436
- ¹¹P. C. Khiang, G. Guoxiao, M. B. Chen, and T. H. Lee, *IEEE/ASME Trans. Mechatron.* **11**, 328 (2006). 437
- ¹²G. A. Lesieutre, *Shock Vib. Dig.* **30**, 187 (1998). 438
- ¹³S. O. R. Moheimani, *IEEE Trans. Control Syst. Technol.* **11**, 482 (2003). 439
- ¹⁴S. O. R. Moheimani and Y. K. Yong, *Rev. Sci. Instrum.* **79**, 073702 (2008). 440
- ¹⁵S. O. R. Moheimani, *Rev. Sci. Instrum.* **79**, 071101 (2008). 441
- ¹⁶D. Campolo, R. Sahai, and R. S. Fearing, Proceedings of the IEEE International Conference on Robotics and Automation, Taipei, 2003 (unpublished), Vol. 3, pp. 3339–3346. 442
- ¹⁷Y. Cui, Proceeding of the Sixth World Conference on Intelligent Control and Automation, China, 2006 (unpublished). 443
- ¹⁸J. Agnus and N. Chaillet, INPI Patent No. FR 03000532 (August 2004). 444
- ¹⁹A. J. Fleming and S. O. R. Moheimani, *Rev. Sci. Instrum.* **76**, 073707 (2005). 445
- ²⁰J. G. Smits and W.-S. Choi, *IEEE Trans. Ultrason. Ferroelectr. Freq. Control* **38**, 256 (1991). 446
- ²¹J. Karki, Texas Instr. Appl. Report No. SLOA033A, 2000. 447